ELSEVIER

An investigation of the effect of the particle–fluid and particle–particle interactions on the flow within a hydrocyclone

W. Kraipech [a,*], A. Nowakowski [b], T. Dyakowski [c], A. Suksangpanomrung [d]

[a] *Department of Chemical Engineering, Srinakarinwirot University, Ongkharuk, Nakorn-Nayok 26120, Thailand*
[b] *Department of Mechanical Engineering, University of Sheffield, Mappin Street, Sheffield S13JD, UK*
[c] *Department of Chemical Engineering, UMIST, PO Box 88, Manchester M601QD, UK*
[d] *Department of Mechanical Engineering, Academic Division, Chulachomklao Royal Military Academy, Nakorn-Nayok 26001, Thailand*

Abstract

The effect of the particle–fluid and particle–particle interactions of the flow within a hydrocyclone is investigated. These were studied by applying the time scale analysis. It is shown that the particle–particle interactions, due to the lubrication and collision mechanisms, only play an important role in the vicinity of a hydrocyclone wall, and near the air core. In the remaining region, particle–fluid interactions are dominating. These play a vital role on the separation efficiency as illustrated by the significance of the wakes generated behind larger particles on dragging finer particles.
© 2005 Elsevier B.V. All rights reserved.

Keywords: Particle-fluid interaction; Hydrocyclone; Time-scale analysis

1. Introduction

A hydrocyclone is a type of separation equipment used for solid–liquid and liquid–liquid systems. It is used to separate dispersed particles from a continuous fluid as the effect of a swirl flow, and has been used in many mineral processing and mining industries.

In modelling the hydrocyclone performance, the influence of the particles on the flow is significant, particularly in the dense slurry flow, when the exchange of momentum from the particle–fluid, particle–particle and particle–wall interactions affect the velocity of the fluid. This may cause inefficiency in separation performance. The previous works presented by Bloor and Ingham [3–5], Pericleous and Rhodes [16], Pericleous [15] and Hsieh and Rajamani [10] discounted the effects of the presence of particles on a slurry velocity field by assuming that the flow is diluted (solids concentrate less than 5%), and the particle–fluid interaction for a single particle moving through a liquid without the presence of other particles was applied. However, when solids con-

centrate exceeds 5%, the presence of particles changes the velocity stresses and results in the generation of extra inertial stresses. The constitutive formulae, describing complex particle–fluid and particle–particle interactions are required. Generally, these formulae are very complicated as they take into account the spatial and temporal non-uniformities in the particle distributions as well as the acceleration of relative velocity.

There are two main approaches that can be applied to modelling multi-phase systems. They are a multi-fluid model and particle tracking method. The choice of one particular approach is determined by the character of the predominant interaction between the phases. The purpose of this study is to investigate the method for determining the predominant particle interaction of the flow within a hydrocyclone. From this knowledge, the proper method for modelling particle flow in this separator can be chosen.

In this paper, the equation of motion of a single particle in a fluid, neglecting the presence of other particles, is presented. The influence of neighbouring particles is described. The particle–fluid and particle–particle interactions are analysed using the concept of a time scale analysis introduced by Roco [20]. Here a case study is presented, based on the

* Corresponding author. Tel.: +66 6 999 8908; fax: +66 37 322 608.
E-mail address: wanwilai@swu.ac.th (W. Kraipech).

results published by Rajamani and Milin [17] for a 75 mm hydrocyclone. On this basis, the zones of the predominant interaction mechanism can be defined and in turn, a proper choice of a specific approach for modelling the flow within hydrocyclone can be made. As a result, the complexity of the constitutive formulae describing these interactions might be significantly reduced.

2. Particle–particle interaction related to hydrocyclone performance

In general, the hydrocyclone has been assumed to be operating at a steady state where the classical fluid dynamics can be applied. Stokes' law is generally assumed to be valid in order to develop models because it simplifies the mathematical formulation. Brownian movement, entrance effects on fluid, particle interactions, spinning of particles, curl of the fluid, wall interaction and the effect of turbulent fluctuations, are normally ignored or neglected [22]. The equations describing the separation function (see [8]), are based on an assumption that the particle settling velocity is not affected by the presence of other particles, and that it is a monotonic function of the particle size. In such a case it seems reasonable to assume that the separation process is linear and is a monotonic function of particle diameter. In fact, as the particles move to the wall their concentration increases and the interactions between them start to manifest through the interstitial fluid by secondary currents and pressure field changes. These particle interaction mechanisms cannot be neglected. Recently, Kumar et al. [13] measured the settling velocities for particles in a poly-dispersed mixture. It is obvious that Stokes' law cannot be applied in a study where the particle interactions are considered. Their results show that the motion of large particles is influenced only by the total volume fraction of particles within the system. Therefore, the settling velocity of large particles can be described by the Richardson–Zaki equation [18]. On the other hand, the smaller particles move at almost identical velocities to the larger particles. These small particles appear to be dragged with the larger ones. The settling velocities of small particles are even larger than the corresponding Stokes velocities or those predicted by the existing theories [2] or correlations.

Taneda's [24] experimental results showed that the permanent vortex-ring behind a sphere begins to form in the rear of a sphere when the critical particle Reynolds number, $Re_p = 24$. The size of the vortex-ring increases for higher Reynolds numbers and the wake behind a sphere begins to oscillate at the rear of the permanent vortex-ring when the Reynolds number is about 130. The latest experimental data of Yang et al. [27] and numerical simulations of Tang et al. [25] show how the dispersion of particles in a wake is organised for small Stokes number particles. Particles with Stokes number less than 1 are able to respond to the small-scale flow pattern and therefore become essentially flow-tracers. The trajecto-
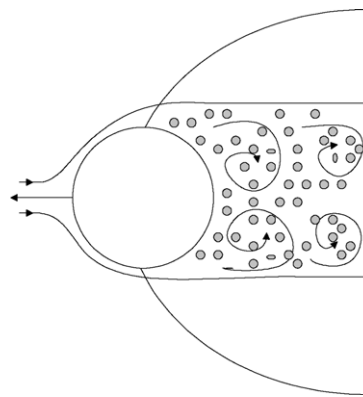

Fig. 1. Dragged mechanism of fine particles by large particle.

ries of these particles distribute themselves throughout the large-scale vortex cores. Conversely particles with a Stokes number much greater than 1 are little affected by the fluid fluctuations at any scale and therefore simply move in the direction of their initial trajectories with only slight deviation.

The ratio between the centrifugal acceleration, w^2/r, and the gravitational acceleration, g, varies along the hydrocyclone radius. The tangential velocity reaches its peak near the hydrocyclone axis. According to Cilliers [6], for a 10 mm
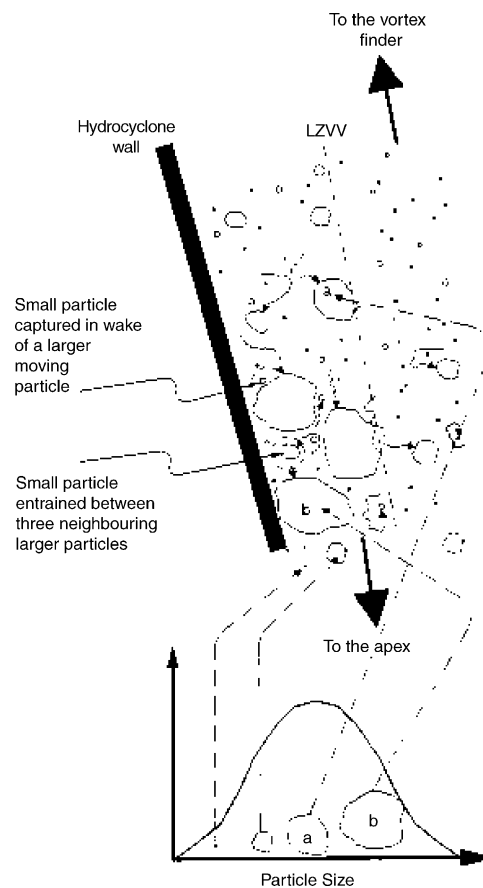

Fig. 2. Mechanisms that describe the fish–hook phenomenon (Roldan-Villasana [21]).

diameter hydrocyclone, the ratio between the centrifugal and gravitational acceleration is around 60,000 and the particle residence time is in the order of milliseconds. These are extreme conditions in relation to the gravitational buoyancy-driven separation of the dispersed phase from the continuous phase.

Therefore, interactions similar to those predicted by Yang et al. [27], and caused by the presence of the vortex-ring behind particles, seems to be worthy of consideration in terms of hydrocyclone performance. These can provide an additional mechanism for finer particles reporting to the underflow in the wake behind the larger particles (see Fig. 1). Such a mechanism may explain the shape of the selectivity curve, and the fact that the bypass value is higher than the water recovery to the underflow. This selectivity curve does not have a sigmoidal shape, but exhibits a dip in regions of finer particle size. This dip is known as the fish–hook effect. The methods of modelling the fish–hook effect of the flow within hydrocyclones, based on this mechanism, were investigated by Kraipech et al. [12].

The hydrodynamic behaviour of hydrocyclones treating concentrated slurries has yet to be fully understood and no accurate theory exists to simulate the phenomena occurring within hydrocyclones. Therefore, the other mechanisms explaining the fish–hook effect proposed by previous researchers such as Roldan-Villasana et al. [22] and Frachon and Cilliers [9], who introduced the idea of an influence from the turbulent dispersion on the motion of fine particles, could

be possible and should not be dismissed. Fig. 2 illustrates the possible mechanisms that describe the fish–hook phenomenon.

3. Equation of particle motion

The equation of motion of a spherical particle in a fluid, neglecting the interactions with other particles can be written as [1]:

$$m_p \frac{d\mathbf{u}_p}{dt} = m_p \left(1 - \frac{\rho}{\rho_p} \right) \mathbf{g} + \mathbf{F}_D + \mathbf{F}_{App} + \mathbf{F}_{Bas} + \mathbf{F}_{LS}$$
$$+ \mathbf{F}_{LM} + \mathbf{F}_{PG} \qquad (1)$$

where m_p is the mass of the particle, $\mathbf{u}_p$ the instantaneous velocity of the particle and $\mathbf{g}$ the body acceleration. ρ and ρ_p are the densities of fluid and solid particles, respectively.

The term on the left-hand side of Eq. (1) describes the particle inertia, and the terms on the right-hand side are the forces caused by the particle–fluid interactions as explained in Table 1. When a particle's motion is affected by a neighbouring particle the other forces have to be altered as shown in Table 2.

There are two main causes for lateral lift force on a particle: one is due to the rotation of a particle moving in a fluid, and another is due to the shear of fluid itself, that is, the shear flow induces the lateral lift force even if the rotation of the

Table 1
Forces caused by particle–fluid interactions of a particle flow in a turbulent fluid

Forces	Sources of forces	Equations		
Steady-state drag force, $\mathbf{F}_D$	The force acts on a particle in order to move the particle through a fluid with a uniform pressure and velocity field when there is no acceleration of the relative velocity between the particle and the conveying fluid	$\mathbf{F}_D = \frac{1}{2}\rho C_D \frac{\pi d^2}{4} |\mathbf{u} - \mathbf{u}_p|(\mathbf{u} - \mathbf{u}_p)$	(4)	d is the particle diameter, $(\mathbf{u} - \mathbf{u}_p)$ the relative velocity between fluid and particle and C_D the drag coefficient
Added mass force, $\mathbf{F}_{App}$	The force of the particle on the fluid due to the acceleration of the relative velocity. When a particle is accelerated through the fluid, there is a corresponding acceleration of the fluid, which is at the expense of work done by the particle. This additional work causes the added mass force, which is required to accelerate the surrounding fluid	$\mathbf{F}_{App} = \frac{\rho V_p}{2} \left(\frac{d\mathbf{u}}{dt} - \frac{d\mathbf{u}_p}{dt} \right)$	(5)	V_p is the particle volume and $\left(\frac{d\mathbf{u}}{dt} - \frac{d\mathbf{u}_p}{dt} \right)$ is the relative acceleration of the fluid with respect to the particle acceleration
Basset force, $\mathbf{F}_{Bas}$	The force due to the temporal delay in the boundary layer around the particle development as the relative velocity changes with time. This force takes into account the viscous effects due to the acceleration of the relative velocity	$\mathbf{F}_{Bas} = \frac{3}{2}d^2 \sqrt{\pi\rho\mu} \int_{t_0}^{t} \frac{(d\mathbf{u}/dt)-(d\mathbf{u}_p/dt)}{\sqrt{t-t'}} dt'$	(6)	
Saffman lift force, $\mathbf{F}_{LS}$	The force produced by the pressure distribution developed on a particle due to the rotation induced by a fluid velocity gradient	$\mathbf{F}_{LS} = 1.615d^2(\mu\rho\dot{\gamma})^{1/2}(\mathbf{u} - \mathbf{u}_p)$	(7)	$\dot{\gamma}$ is the rate of fluid deformation
Magnus lift forces, $\mathbf{F}_{LM}$	The force due to the rotation of the particle. This force is caused by a pressure difference between both sides of the particle resulting from the velocity difference due to the rotation	$\mathbf{F}_{LM} = \frac{1}{2}\rho(\mathbf{u} - \mathbf{u}_p)^2 C_L \frac{\pi d^2}{4}$	(8)	C_L is the lift force coefficient
Pressure gradient force, $\mathbf{F}_{PG}$	The force due to the pressure gradient in the fluid surrounding the particle	$\mathbf{F}_{PG} = -V_p \nabla p$	(9)	

Table 2
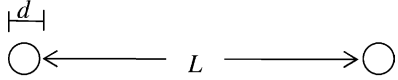The effect of neighbouring particles on the particle motion

Distance between particles, L	Flow mechanism	Flow diagram
$\frac{L}{d} > 10$	No interaction between particles	
$\frac{L}{d} \approx 2$	Vortex shedding	
$\frac{L}{d} \approx 0.5$	Lubrication	
$\frac{L}{d} = 0$	Collision	

Table 3
Time scales for particle interactions in the hydrodynamic range [20]

Type of particle interaction	Time scale, t_m		Comments
Liquid–solid interaction (drag)	$t_d = \frac{4}{3}\frac{sd}{C_D|\mathbf{u}-\mathbf{u}_p|}$	(10)	$C_D = f(Re_p)$, Re_p is the particle Reynolds number
Lubrication	$t_{lub} = \frac{18}{s}\frac{\lambda}{\dot{\gamma}_{ij}}$	(11)	$\lambda = \frac{1-(\alpha^*)^{0.33}}{(\alpha^*)^{0.33}}$, where $\alpha^* = \frac{\alpha}{\alpha_{max}}$
Collision	$t_{col} = \frac{45}{s\dot{\gamma}_{ij}} + \frac{4.5}{s\dot{\gamma}_{ij}}\ln(\lambda)$	(12)	The first term on the right-hand side corresponds to the particle roughness

particle is absent. The former is called the Magnus effect and the latter is the Saffman effect, which are additionally described in Table 1. The Saffman lift force is predominantly induced when a solid particle moves in a region with a shear flow of a steep velocity gradient in the surrounding fluid. When the rotation of a particle is given from the beginning of the transport, the Magnus lift force is predominant.

Dense flow is characterised by high collision frequencies between particles, and hence their motion is dominantly influenced by particle–particle collisions. Interactions between the fluid and particles are of minor importance [23]. The models for predicting the collision forces are not discussed here but they can be found in the references of Crowe et al. [7], Tsirkunov and Panfilov [26] and Sommerfeld [23]. Generally speaking, the collision force depends on the properties of the particles such as density and surface roughness, as well as on the magnitude and the direction of the relative velocity.

The lubrication interaction is the particle–particle interaction due to the pressure in a fluid, which is generated by the particles approaching each other. This pressure can be calculated using the lubrication theory, which neglects all inertial forces in a fluid (creeping flow approach). By integrating this pressure distribution along the particle surface, an additional force, the lubrication force, acting on the particle can be derived [7]. Assuming that the flow is symmetrical about the centre plane between two, this force can be described by the following equation:

$$F_{Lub} = -\frac{3\pi\mu d^2\dot{h}}{8h_0} \qquad (2)$$

where h_0 is the distance between the sphere and the symmetric plane, which is perpendicular to the plane, and $\dot{h}$ the rate at which the sphere is approaching the symmetric plane.

4. Time scale analysis

The frequency of an interaction mechanism's occurrence between particles, or between particles and fluid, is inversely proportional to the time required by the particle to respond to the interaction mechanism.

An interaction mechanism "n" that is characterised by the time scale t_n is more frequent and therefore has a larger distribution to the momentum transfer than another interaction mechanism "m" characterised by the time scale t_m, if $t_n < t_m$. This relation is defined as the relative particle interaction

Table 4
Relative particle interaction number, $N_{n,m}$ [20]

Relative interaction mechanisms	Significant ratio	Relative particle interaction number	
Particle–particle lubrication/particle–liquid drag	$\frac{t_d}{t_{lub}}$	$N_{d,lub} = \frac{s^2 d^2 \dot{\gamma}_{ij}}{18^2 v\lambda}$	(13)
Particle–particle collisions/particle–liquid drag	$\frac{t_d}{t_{col}}$	$N_{d,col} = \frac{s^2 d^2 \dot{\gamma}_{ij}}{18v}\frac{1}{45+4.5\ln(\lambda)}$	(14)
Particle–particle collisions/particle–particle lubrication	$\frac{t_{lub}}{t_{col}}$	$N_{lub,col} = \frac{18\lambda}{45+4.5\ln(\lambda)}$	(15)

Note: t_d is replaced by its expression for the Stokesian ($Re_p \leq 0.1$) in this table.
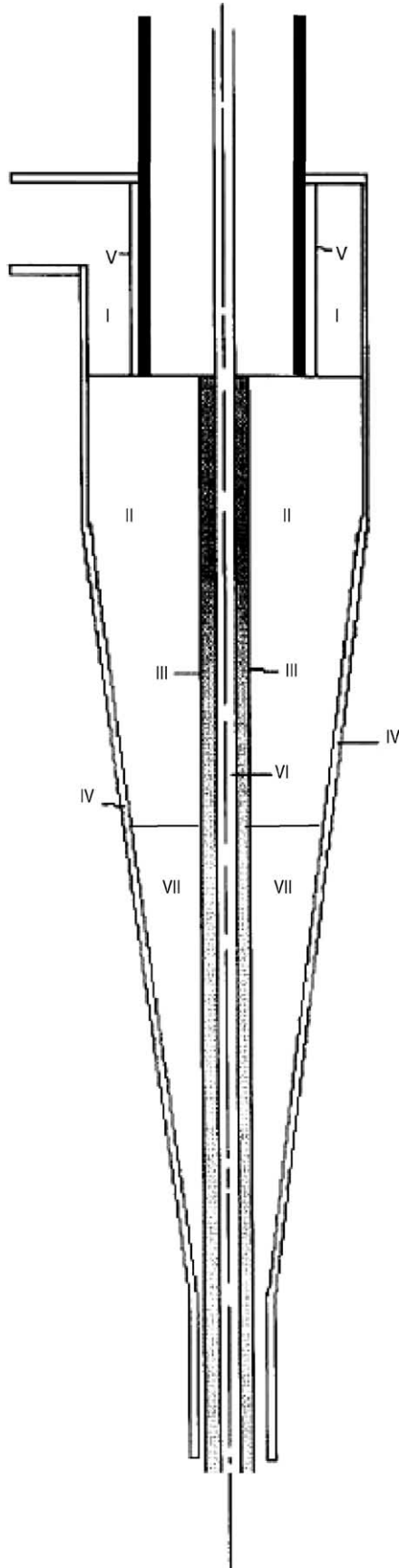
Fig. 3. Zones in the hydrocyclone.

number, $N_{n,m}$.

$$\frac{1/t_m}{1/t_n} = \frac{t_n}{t_m} = N_{n,m} \tag{3}$$

If $N_{n,m} < 1$, the nth mechanism is prevalent comparative to the mth mechanism.

The time scales responding to liquid–solid (drag), lubrication and collision interactions and the relative particle interaction numbers $N_{n,m}$, are shown in Tables 3 and 4, respectively. They were derived using a similar method as discussed by Roco [19] (see [11]). On the contrary to the drag time scale, the lubrication and collision time scales are dependent on the velocity profile and the solids volume fraction.

5. A case study for calculating the time scales of the flow within a hydrocyclone

In this study, an application of a time scale analysis to identify the predominant interaction is presented for the 75 mm hydrocyclone, based on the experiment and prediction of Rajamani and Milin [17]. The time scales are calculated for seven flow zones within a hydrocyclone, instead of six flow zones, which was carried out in the author's previous work,

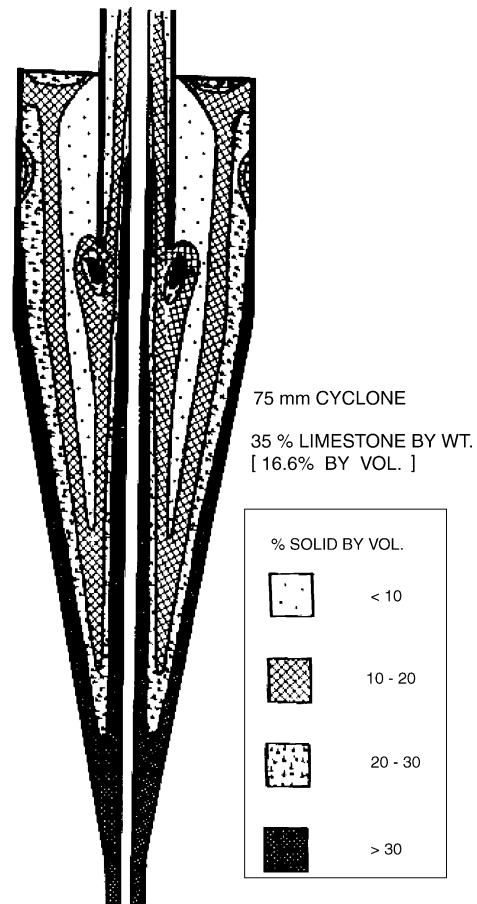75 mm CYCLONE

35 % LIMESTONE BY WT.
[16.6% BY VOL.]

% SOLID BY VOL.	
	< 10
	10 - 20
	20 - 30
	> 30

Fig. 4. Predicted volumetric concentration map for 35% limestone by weight (16.6% by volume) in the feed [17].

Table 5
Location of zones

Zone	Location
I	The upper cylindrical part of the hydrocyclone, from the top to the bottom of the vortex finder tube, outside the boundary layer on the outer wall of the vortex finder. Because of the high level of turbulence and secondary flows that originate due to the tangential entrance, the flow is well mixed containing a homogeneous suspension
II	The middle part of the hydrocyclone from the bottom of the vortex finder tube to the middle of the conical section outside the boundary layer on the lateral walls and the boundary layer near the air core
III	The area near the air core
IV	The boundary layer on the lateral walls. The boundary layer starts at the feed and develops its maximum thickness when reaching the level of the bottom of the vortex finder tube
V	The boundary layer at the outer wall of the vortex finder
VI	The air core, which is assumed to have a cylindrical shape
VII	The lower part of the hydrocyclone from the middle to the end of the conical section outside the boundary layer on the lateral walls and the boundary layer near the air core

Table 6
The experimental selectivity values [17]

Particle size (μm)	Percent of solid recovery to underflow
90	100
65	92
45	80
33	52
23	30
16	20
11	16
8	11
4	10
3	9
1	7

Kraipech [11]. The locations of each zone are described and shown in Table 5 and Fig. 3.

The feed slurry of the case study is 35% by weight of limestone (16.6% by volume). The liquid phase is water, which has a density of 1000 kg/m^3 and a kinematic viscosity of 10^{-6} m^2/s. The density of limestone is 2700 kg/m^3 and its volume fraction at maximum packing is 0.7. The particle size is in the range of 1–90 μm (Table 6). The volumetric concentration map and tangential velocity profile are shown in Figs. 4 and 5, respectively.

The time scales and their relative particle interaction numbers are the functions of flow data such as the velocity field, particle sizes and the solid concentration, as shown in Tables 3 and 4. Therefore, it is possible to calculate the time scales and their relative particle interaction numbers for a given set of data describing the flow.

Fig. 5. Measured and predicted tangential velocities in a 75 mm hydrocyclone [17].

Table 7
The flow characteristics in each zone in the hydrocyclone

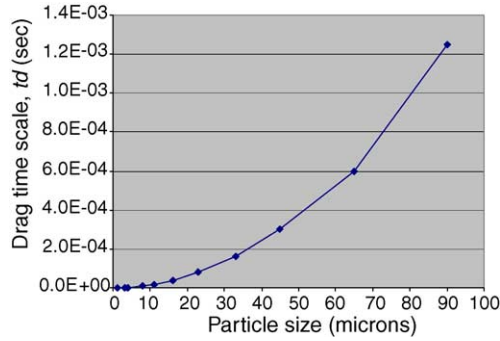| Zone	Volume fraction, α	Particle size (μm)	The mean rate of strain tensor, $\lvert \dot{\gamma}_{r\theta} \rvert = \frac{r}{2} \left\lvert \frac{\partial}{\partial r} \left(\frac{w}{r} \right) \right\rvert$ (s^{-1})
I	$\alpha < 0.1$; $0.1 < \alpha < 0.2$; $0.2 < \alpha \leq 0.3$	1–90	107
II	$\alpha < 0.1$; $0.1 < \alpha < 0.2$; $0.2 < \alpha \leq 0.3$	1–90	110
III	$\alpha > 0.3$	1–90	570
IV	$\alpha > 0.3$	1–90	179
V	$\alpha < 0.1$	1–65	19
VI	–	–	–
VII	$\alpha < 0.1$; $0.1 < \alpha < 0.2$; $0.2 < \alpha \leq 0.3$	1–90	187

Fig. 6. Drag time scale, t_d, of the limestone particle flow in water (kinematic viscosity of 10^{-6} m^2/s) obtained from the experimental results of Rajamani and Milin [17].

Eqs. (10)–(12) are used to calculate the drag, lubrication and collision time scale. The flow around the particle is assumed to be in the Stokes' law region. Therefore, $C_D = \frac{24}{Re_p}$. The aqueous suspension of limestone is assumed to be a Newtonian fluid for all range of weigh fraction in order to simplify the calculation, even though the suspension shows a non-Newtonian behaviour when its weight fraction is high. The rate of strain tensor can be calculated from the tangential velocity profile, which is presented in Fig. 5. The component $\dot{\gamma}_{r\theta} = \frac{r}{2} \frac{\partial}{\partial r} \left(\frac{w}{r} \right) + \frac{1}{2r} \frac{\partial v}{\partial \theta}$ of the rate of strain tensor is taken into this analysis, instead of $\dot{\gamma}_{r\theta} = \frac{\partial w}{\partial r}$ which is used in Nowakowski et al. [14]. Assuming that the flow is axisymmetrical, the term $\frac{1}{2r} \frac{\partial v}{\partial \theta}$ is neglected. The absolute value of the rate of strain tensor can be calculated as $|\dot{\gamma}_{r\theta}| = \frac{r}{2} \left| \frac{\partial}{\partial r} \left(\frac{w}{r} \right) \right|$. The ratio between the inter-particle distance and the particle diameter, λ, is equal to $\frac{1 - (\alpha^*)^{0.33}}{(\alpha^*)^{0.33}}$, where $\alpha^* = \frac{\alpha}{\alpha_{max}}$. α_{max} is the solids volume fraction at maximum packing and α the solids volume fraction obtained from the volumetric concentration as shown in Fig. 4. In this figure, the solids concentration distribution is presented in three ranges of volumetric concentration. According to the experimental results, it is assumed that there are no particles equal to or larger than 90 μm in diameter in Zone V (see Fig. 3). The flow characteristics are summarised in Table 7. The drag time scale as a function of the particle diameter is shown in Fig. 6. The time scales
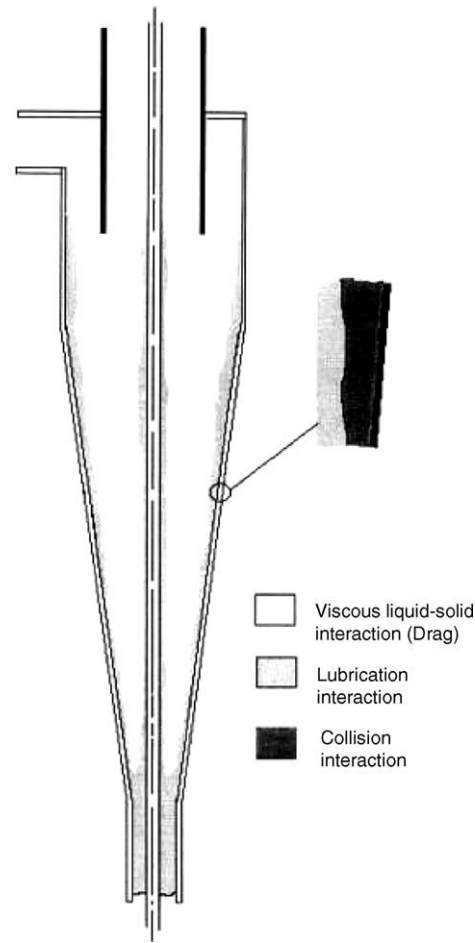

Fig. 7. Main particle interaction mechanisms in the 75 mm hydrocyclone.

for lubrication and collision interactions are presented in Table 8.

Fig. 6 shows that an increase in the particle size leads to an increase in the drag time scale, since a larger particle needs more time to respond to the change in fluid velocity than a smaller one. The lubrication and collision time scales decrease with an increase in the solids volume fraction and the mean rate of strain tensor. This indicates that these two

Table 8
Lubrication time scale, t_{lub}, and collision time scales, t_{col}

Zone	Solid concentration (volume fraction)	$t_{lub} = \frac{18}{s} \frac{\lambda}{\dot{\gamma}_{ij}}$ (s)	$t_{col} = \frac{45}{s\dot{\gamma}_{ij}} + \frac{4.5}{s\dot{\gamma}_{ij}} \ln(\lambda)$ (s)
I	$\alpha < 0.1$; $0.1 < \alpha < 0.2$; $0.2 < \alpha \leq 0.3$	$t_{lub} > 0.0561$; $0.0561 > t_{lub} > 0.0319$; $0.0319 > t_{lub} \geq 0.0201$	$t_{col} > 0.0952$; $0.0952 > t_{col} > 0.0864$; $0.0864 > t_{col} \geq 0.0792$
II	$\alpha < 0.1$; $0.1 < \alpha < 0.2$; $0.2 < \alpha \leq 0.3$	$t_{lub} > 0.0546$; $0.0546 > t_{lub} > 0.0319$; $0.0319 > t_{lub} \geq 0.0201$	$t_{col} > 0.0926$; $0.0926 > t_{col} > 0.084$; $00.0840 > t_{col} \geq 0.0770$
III	$\alpha > 0.3$	$t_{lub} < 0.0037$	$t_{col} < 0.0149$
IV	$\alpha > 0.3$	$t_{lub} < 0.0120$	$t_{col} < 0.0473$
V	$\alpha < 0.1$	$t_{lub} > 0.0316$	$t_{col} > 0.0536$
VI	–	–	–
VII	$\alpha < 0.1$; $0.1 < \alpha < 0.2$; $0.2 < \alpha \leq 0.3$	$t_{lub} > 0.0321 0.0321 > t_{lub} > 0.0183 0.0183 > t_{lub} \geq 0.0115$	$t_{col} > 0.0545 0.0545 > t_{col} > 0.0494 0.0494 > t_{col} \geq 0.0453$

Table 9
Prevalent interaction mechanism for each flow zone in the hydrocyclone

Zone	Solid concentration condition	Relative particle interaction numbers			Prevalent particle interaction mechanism
		$N_{d,lub}$	$N_{d,col}$	$N_{lub,col}$	
I	$\alpha \leq 0.3$	$N_{d,lub} < 1$	$N_{d,col} < 1$	$N_{lub,col} < 1$	Liquid–solid interaction (drag)
II	$\alpha \leq 0.3$	$N_{d,lub} < 1$	$N_{d,col} < 1$	$N_{lub,col} < 1$	Liquid–solid interaction (drag)
III	$0.3 < \alpha < 0.52$	$N_{d,lub} < 1$	$N_{d,col} < 1$	$N_{lub,col} < 1$	Liquid–solid interaction (drag)
	$\alpha \geq 0.52$	$N_{d,lub} > 1$	$N_{d,col} < 1$	$N_{lub,col} < 1$	Lubrication interaction
IV	$0.3 < \alpha < 0.64$	$N_{d,lub} < 1$	$N_{d,col} < 1$	$N_{lub,col} < 1$	Liquid–solid interaction (drag)
	$\alpha \geq 0.64$	$N_{d,lub} > 1$	$N_{d,col} < 1$	$N_{lub,col} < 1$	Lubrication interaction
V	$\alpha < 0.1$	$N_{d,lub} < 1$	$N_{d,col} < 1$	$N_{lub,col} < 1$	Liquid–solid interaction (drag)
VI	–	–	–	–	–
VII	$\alpha \leq 0.3$	$N_{d,lub} < 1$	$N_{d,col} < 1$	$N_{lub,col} < 1$	Liquid–solid interaction (drag)

mechanisms are not only dependent on the flow concentration but also on the flow velocity field. The prevalent interaction mechanisms in each flow zone are determined by using the data shown in Fig. 6 and Table 8, and are presented in Table 9 and Fig. 7.

From this analysis, it is found that for the majority of the area within the hydrocyclone, where the solids concentration is less than 30% by volume, the main particle interaction mechanism is the liquid–solid interaction (drag). In the high solids concentration areas, the lateral boundary layer (zone IV) and the area near the air core (zone III), the lubrication and collision interaction mechanisms are prevalent compared with the drag interaction mechanisms. This is in agreement with the work of Nowakowski et al. [14].

6. Conclusion

An application of a qualitative analysis based on a "time scale" concept was presented and discussed to assess the predominant interaction mechanisms within a hydrocyclone. It was found that the liquid–particle interaction (drag) plays an important role in the main body of a hydrocyclone. However, within the regions close to the walls and the air core, both lubrication and collision mechanisms are predominant. This means that the flow pattern within a hydrocyclone should not only be described by interactions between particles and carrying fluid but that the results of solid mechanics should also be included in modelling particle–particle collisions in the vicinity of the hydrocyclone walls. The future work should lead to deriving a simplified model for the particle transport taking into account only the dominating relevant forces in each region. The extension of the analysis to the non-Newtonian behaviour of the high weight fraction of limestone suspensions is also planned.

Acknowledgement

References

[1] M.K. Akbar, M.A.R. Sharif, R.C. Bradt, Effect of forces on a particle in a straight channel turbulent flow, in: Proceedings of the Fourth International Conference on Multiphase Flow, vol. 53, New Orleans, LA, USA, May 27–June 1, Institution of Chemical Engineers, 2001, pp. 1–6.

[2] G.K. Batchelor, Sedimentation in a dilute polydisperse system of interacting sphere. Part 1. General theory, J. Fluid Mech. 119 (1982) 372–408.

[3] M.I. Bloor, D.B. Ingham, Theoretical investigation of the flow in a conical, Trans. Inst. Chem. Eng. 51 (1973) 36–41.

[4] M.I. Bloor, D.B. Ingham, Turbulent spin in a hydrocyclone, Trans. Inst. Chem. Eng. 53 (1975) 1–6.

[5] M.I. Bloor, D.B. Ingham, The flow in industrial cyclones, J. Fluid Mech. 178 (1987) 507–519.

[6] J.J. Cilliers, Private communication, 2001.

[7] C.T. Crowe, M. Sommerfeld, Y. Tsuji, Multiphase Flows with Droplets and Particles, CRC Press, USA, 1998.

[8] B.C. Flintoff, L.R. Plitt, A.A. Turak, Cyclone modelling a review of present technologies, CIM Bull. 80 (1987) 39–50.

[9] M. Frachon, J.J. Cilliers, A general model for hydrocyclone partition curves, Chem. Eng. J. 73 (1999) 53–59.

[10] K.T. Hsieh, R.K. Rajamani, Mathematical model of hydrocyclone based on physics of fluid flow, AIChE J. 37 (5) (1991) 735–745.

[11] W. Kraipech, Studying the performance of mineral hydrocyclones, Ph.D. Thesis, University of Manchester, Institute of Science and Technology, 2002.

[12] W. Kraipech, W. Chen, F. Parma, T. Dyakowski, Modelling the fish–hook effect of the flow within hydrocyclones, Int. J. Miner. Process. 66 (2002) 49–65.

[13] S. Kumar, T.W. Pirog, D. Ramkrishna, A new method for estimating hindered creaming/settling velocity of particles in polydisperse systems, Chem. Eng. Sci. 55 (2000) 1893–1904.

[14] A. Nowakowski, W. Kraipech, T. Dyakowski, R. Williams, The hydrodynamics of a hydrocyclone based on a three-dimensional multi-continuum model, Chem. Eng. J. 80 (2000) 275–282.

[15] Pericleous, Mathematical simulation of hydrocyclones, Appl. Math. Model. 11 (1987) 242–255.

[16] K.A. Pericleous, N. Rhodes, The hydrocyclone classifier: a numerical approach, Int. J. Miner. Process. 17 (1986) 23–43.

[17] R.K. Rajamani, L. Milin, Fluid-flow model of the hydrocyclone for concentrated slurry classification, in: L. Savarovsky, M.T. Thew (Eds.), Hydrocyclone Analysis and Applications, Kluwer Academic Publishers, London, 1992, pp. 59–108.

[18] J.F. Richardson, W.N. Zaki, Sedimentation and fluidisation, Part 1, Trans. Inst. Chem. Eng. 32 (1954) 35–53.

[19] M.C. Roco, Dense slurry flow, in: Proceedings of the Advancement in Aerodynamics, Fluid Mechanics and Hydraulics, ASCE, EM & HY Div., 1986, pp. 365–376.

[20] M.C. Roco, Turbulent flow of incompressible mixtures, in: Encyclopedia of Fluid Mechanics, vol. 10, Gulf Publisher Company, Houston, TX, 1990, pp. 1–68.

[21] E.J. Roldan-Villasana, Modelling and Simulation of Hydrocyclone Networks for Fine Particle Processing, Ph.D. Thesis, UMIST, Manchester, UK.

[22] E.J. Roldan-Villasana, R.A. Williams, T. Dyakowski, The origin of the fish–hook effect in hydrocyclone separators, Powder Technol. 77 (1993) 245–250.

[23] M. Sommerfeld, Validation of a stochastic Lagrangian modelling approach for inter-particle collisions in homogeneous isotropic turbulence, Int. J. Multiphase Flow 27 (2001) 1829–1858.

[24] S. Taneda, Studies on wake vortices (III): experimental investigation of the wake behind a sphere at low Reynolds numbers, Rep. Res. Inst. Appl. Mech. IV 16 (1956) 99–105.

[25] L. Tang, F. Wen, Y. Yang, C.T. Crowe, J.N. Chung, T.R. Troutt, Self-organizing particle dispersion mechanism in a plane wake, Phys. Fluids A4 10 (1992) 2244–2251.

[26] Y.M. Tsirkunov, S.V. Panfilov, Modelling of particle–wall interaction in two-phases flows at moderate and high particle impact velocity, in: Proceedings of the Third International Conference on Multiphase Flow, ICMF 98, Lyon, France, June 8–12, 1998.

[27] Y. Yang, C.T. Crowe, J.N. Chung, T.R. Troutt, Experiments on particle dispersion in a plane wake, Int. J. Multiphase Flow 26 (2000) 1583–1607.